Nanosecond-pulsed discharges in liquids for nanoobject synthesis: expectations and capabilities

A. V. Nominé[1], V. Milichko[1,2], A. Nominé[1], C. Noël[1], Th. Gries[1], T. Belmonte[1]

[1] *University of Lorraine, CNRS, IJL, F-54000 Nancy, France*
[2] *Department of Nanophotonics and Metamaterials, ITMO University, St. Petersburg, 197101, Russia*

Abstract: Nanosecond-pulsed discharges in liquids are capable of synthesizing nano-objects made of new phases or complex arrangement of phases with unique properties but they are also expected to be more selective in size distribution, shape design and composition mastering. Taking benefit from the non-equilibrium conditions that are created in these media, these processes thus open new perspectives. The example of the synthesis of nano-objects made of Si, Au, La, Fe and O is used in this work to illustrate expectations and capabilities of discharges in liquids.

Keywords: Discharges in liquids, nano-objects.

1. Introduction

Nanosecond- pulsed discharges in liquids are commonly used to produce different kinds of nano-objects by electrode erosion [1–3].

In a recent study [4], the formation of alloyed nanocrystals made of Ag and Cu, two non-miscible elements, was proved to be effective. However, these nanoparticles have broad size distributions. Additional laser post-treatment contributes to improving these drawbacks as it results in an increase in size of the small particles along with a decrease in size of large particles and subsequent narrowing of the size distribution. The EDS mapping shows the uniform distribution of the metallic elements in the nanoparticles (NP), which is indicative of alloyed-NP formation. Segregation of both elements may still exist but at a resolution that could not be reached in these 3D nanospheres whose radius stands around 20-30 nm. These alloyed-NP demonstrate plasmon-induced scattering of light in the 560–640-nm region. The treatment transforms the turbid and colourless solution into a solution with well-defined absorption of the yellow-orange light (550–600 nm).

Applying this process to the Au-Si system enabled the production of plasmonic nanosponges [5]. In this case, even though the two elements do not mix, they get distributed in a way that leads to new behaviours. When a gold thin network separates high-refractive index nanocrystals (*e.g.* Si, Ge, GaP, etc.), nonlinear optical effects are strongly enhanced. In the case of Au and Si, these hybrid NPs are constituted of a gold sponge-like structure filled with Si nanocrystals. The Au matrix provides strong near-field enhancement in the Si grains, increasing white light photoluminescence in the hybrid nanostructures compared to uniform Si nanoparticles.

In this work, we investigate the substitution of all or part of Si in the previous system by a perovskite: $LaFeO_3$. This material exhibits both catalytic and optical properties that could be used for water splitting for instance [6]. The possibility of controlling the concentrations of the various elements and of designing the shape of the NP is a mid-term objective that this first attempt initiates.

2. Experimental setup

The experimental setup was presented in detail elsewhere [2]. Succinctly, a solid-state switch (Behlke HTS-301-03-GSM), supplied by a high DC voltage power generator (Technix SR15-R-1200–15 kV–80 mA) was connected to a plate electrode, the other pin electrode being grounded. This set was immersed in liquid nitrogen. The voltage rise time is close to 20 ns.

A pin-to-plate arrangement was necessary as the simplest way to get a plate electrode made of Au, La and Fe was by sputtering on a (001)-oriented silicon wafer. The thus-produced stack is showed in **Fig. 1**. The pin electrode was made of W (99.9% purity) and conically sharpened to reach curvature radii around 100 nm.

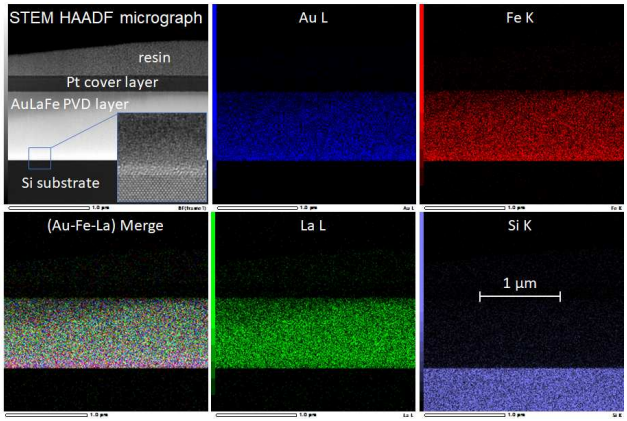

Fig. 1: Amorphous AuFeLa PVD coating (880 nm thick) deposited onto Si. Insert in the STEM HAADF micrograph is a high-resolution image of the Si-coating interface. EDX analysis gives the following atomic composition: 30% Au, 36% Fe, 34% La.

Discharges were pulsed at 10 Hz for 30 min. The influence of the positive voltage (+4, 5, 7, and 10 kV) applied to the biased electrode was studied. The discharge pulse width, whose duration affects only the amount of synthesized nanoparticles, was 75 ns. The inter-electrode gap distance was 100 µm.

Nano-objects were collected on a silicon wafer laid on the bottom of a Dewar vessel. After treatment, nitrogen was evaporated and nano-objects were transferred to a holey carbon grid before TEM analyses by rubbing the silicon surface. NPs were characterized by high-resolution transmission electron microscopy (HRTEM) to determine their structure and composition. A JEOL ARM 200F cold FEG TEM/ STEM, equipped with a GIF quantum ER model 965, was operated at 200 kV (point resolution: 0.078 nm in STEM mode). High-angle annular dark-field scanning transmission electron microscopy (HAADF-STEM) and two-dimensional elemental mapping using energy-dispersive X-ray spectroscopy (EDX) were combined to determine the chemical composition of NPs.

3. Results and discussion

In **Fig. 2**, three types of particles (~140, 220 and 250 nm in diameter) are depicted. The atomic compositions of particles 2a and 2b are quite similar (see **Table 1**). Particle 2c is depleted in silicon and lanthanum and richer in iron. No tungsten, from the pin electrode, was ever found in the formed NPs, at least within the accuracy of the performed EDX measurements.

Table 1. Atomic compositions of selected particles.

	Si	Fe	La	Au	O
Particle 2a	25%	16%	28%	20%	11%
Particle 2b	29%	21%	15%	23%	12%
Particle 2c	9%	43%	7%	24%	17%

The most striking feature of particle 2a is its homogeneity. In **Fig. 2a**, the particle composition is highly homogeneous in Si, Au, Fe and La. Especially, it is not possible to observe any segregation between iron and gold, at least with a resolution of 3 nm maximum. The distribution of oxygen is however not homogenous, which suggests some minor (*i.e.* < 5 nm as showed by the oxygen map in **Fig. 2a**) surface segregation driven by oxidation after objects are removed from liquid nitrogen and exposed to air. However, for this very small particle, it is not simple to correlate the oxygen signal with that Si, Fe or La.

Particle 2b exhibits a segregated structure, where Au and Fe are split over domains larger than 8 nm. Spots of either element do not overlap. It is also true for lanthanum and silicon that are distributed differently. By the way, surface depletion in La is quite visible. This explains why the oxygen EDX intensity correlates relatively well with those of silicon and iron. However, the respective contributions of each element, Si and Fe, are not easy to evaluate.

The main difference between particles 2a and 2b and particle 2c is the presence of an open porosity, due to aggregation of NPs of ~6-9 nm in diameter. This consequently leads to a more homogeneous distribution of oxygen. Indeed, oxygen can diffuse to the core of the porous particles and its distribution is no longer limited to a nanometric shell over the surface of the particle like in the two previous examples. The O signal intensity is even slightly higher in the center where the porosity size is expected to be weaker. Here again, Au and Fe are well split, whereas Si, La and O are more homogeneously distributed, *i.e.* either segregated over smaller domains (below ~3 nm again) or alloyed.

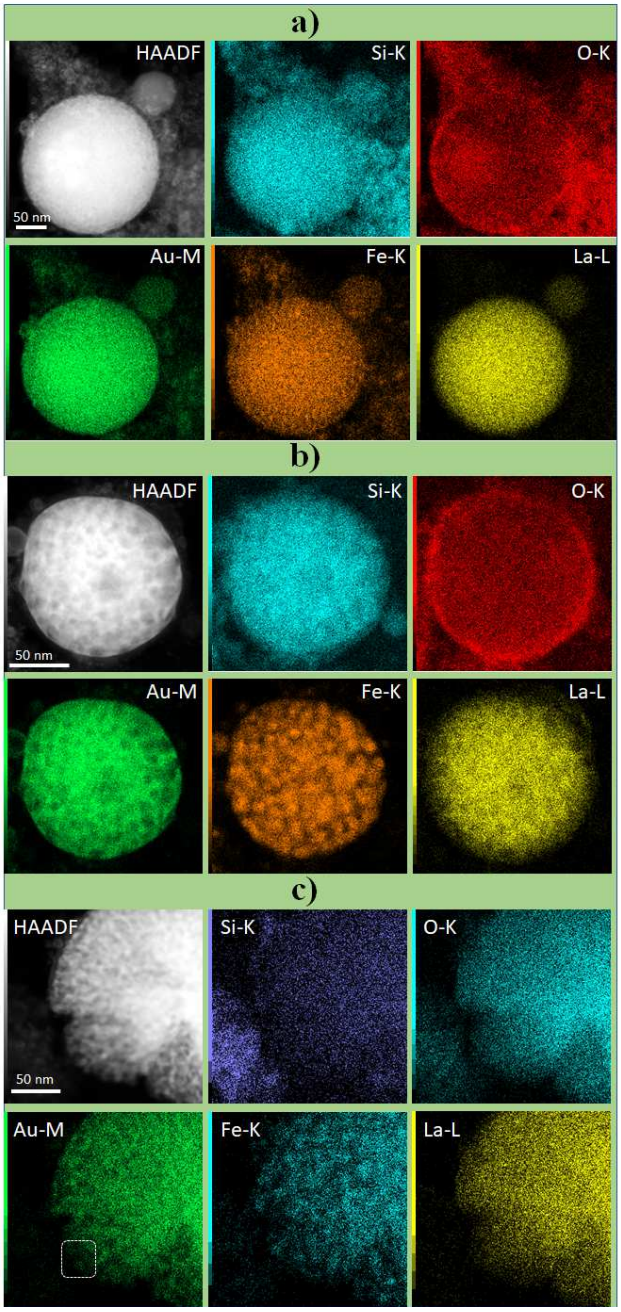

Fig. 2. High-angle annular dark-field image and 2D element maps determined by energy-dispersive X-ray spectroscopy (EDX) are given for a) a homogeneous NP, b) a weakly-segregated NP, c) a porous NP (dotted square corresponds to EELS analysis – see **Fig.3**).

The different oxidation states of these elements can be measured by electron energy-loss spectroscopy (EELS)

measurements. In **Fig. 3**, it is clear that iron and lanthanum are oxidized under the Fe_2O_3 and La_2O_3 states whose footprints match perfectly with experimental data. The lack of silicon signal is either due to the weak content of this element in particle 2c (see **Table 1**) or to the lack of silicon in the outermost region of the particle. This second assumption is however more likely as lanthanum is easily detected (**Fig. 3c**) with a lower nominal content than silicon (see **Table 1**). The signal at the oxygen edge is mainly defined by Fe_2O_3, the La_2O_3 signal being too weak in concentration to pop up in the recorded spectrum. From present results, there is no evidence of features of the $LaFeO_3$ perovskite structure in EELS spectra.

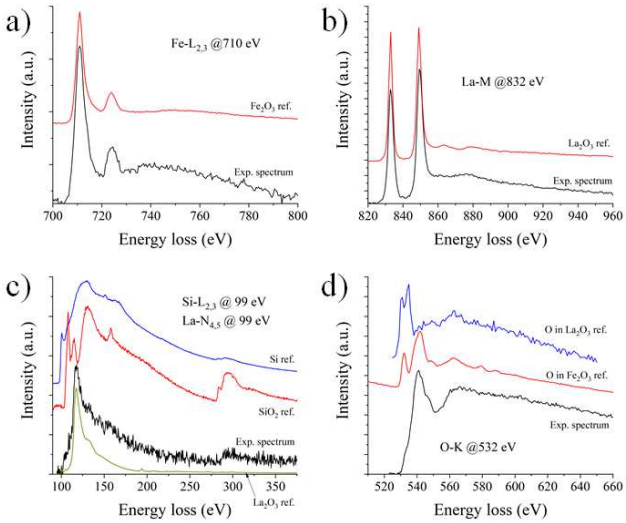

Fig. 3. Main edges (background removed) used in Fe, La, Si and O characterization by electron energy-loss spectroscopy (measurement made on particle 2c). Energy dispersion of 0.5 eV/channel.

At this stage, the main question to be answered is the growth mechanism of these particles. Their segregated structure can be due to the coarsening of smaller particles into larger structures and/or to a heat treatment after synthesis that drives matter to equilibrium.

In **Fig. 4**, an assembly of particles, chained by wires of nanoparticles (~6-9 nm in diameter) are depicted. EDX-elemental maps show a very similar structure to that described in **Fig. 2b**.

The possibility of assembling metallic NPs into 1D structures was explained by Hermanson *et al.* [7]. The assembly is based on the mobility and interactions of particles, caused dielectrophoresis made possible in alternating electric fields. Wire formation is supposed to be a collective effect, where the nanoparticles are at the end of the tip and subsequently aggregate to extend the wire in the direction of the field gradient.

The formation of wires in the present process was explained in a paper by Trad *et al.* [8]. A sufficiently large electric field is needed, which is dependent on the possibility of enhancing the applied electric field by tip effect. When a particle exhibits sharp edges, the curvature radius enhances the electric field and enables an assembly of nanoparticles into a 1D-structure that maintains this field enhancement.

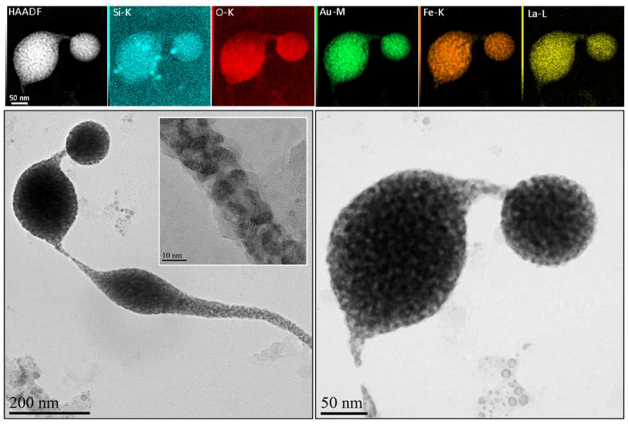

Fig. 4. Top: HAADF image and EDX elemental maps of elongated particles connected by 1D-assembly of particles of ~6-9 nm. Bottom left: larger view of the whole object. Insert: High-resolution image of 1D connection. Bottom right: TEM image showing the porous structure of the assembled particles.

From this observation, it is possible to infer that large particles are obtained by direct assembly of NPs into spheres. Discharges in liquids created with the present process are characterized by the production of 3 size distributions: typically from 1 to 5 nm, from 6 to 24 nm and beyond 100 nm [9]. The last population, formed by ejection of liquid droplets from the molten metal hit by the discharge, is suppressed at sufficiently low applied electric field, which is the case here. The two smallest populations are created by condensation, likely in different part of the discharge, of the vapor emitted by the electrodes.

Agglomeration of either type of nanoparticles into larger structures is assumed to be responsible for the formation of particles of 2a and 2b-2c types. This mechanism is more likely than the emission of liquid droplet as immiscible elements are separated in the liquid phase, like in the case of water and oil. Then, solidification of a liquid mixture, even at ultra-high quenching rate (*i.e.* beyond 10^{10} K s^{-1}), cannot lead to the synthesis of particles 2a.

It is also possible to assume that particles 2a, once synthesized in the discharge, are submitted to further heat treatment. This would separate non-miscible elements into larger domains, leading to particles 2b. There is no way, on the basis of the present data, to know whether this process really occurs. However, if it is does, it is certainly infrequent. Indeed, the possibility of forming a large particle and to treat it thermally afterward within a single discharge is unlikely as the whole discharge process lasts about 1 µs maximum in the present conditions, which is

clearly too short. Synthesis and heat treatment of one particle could be successive, in two different discharges for instance. However, it has documented that once particles are synthesized and transferred into the liquid phase after a single discharge event, they cannot enter the volume of another discharge, being pushed away by the gas-liquid interface during the expansion phase of the bubble [10].

Surface erosion of the plate electrode by the discharge is deep enough to erode fully the AuLaFe PVD layer and partly the silicon substrate. The vapor of the emitted elements condensates in different parts of the gas bubble, forming nanoparticles with two size distributions. Then, nanoparticles get assembled, leading to large particles with different compositions and porosities.

4. Conclusions

Nanosecond-pulsed discharges in liquid nitrogen, created at voltages slightly above the breakdown voltage, produce three populations of nanoparticles, the two smallest being centred at 2-3 nm and 12-15 nm. These two sets of NPs can form, by direct assembly, larger particles with different levels of segregation and porosity.

In the present study, Si, Au, Fe and La can be mixed into submicrometric spherical objects with a resolution typically lower than 3 nm, which likely promotes specific optical or catalytic properties that are yet to be determined, like in the example of Si-Au nanosponges [5]. It is also possible, to a certain extent, to create an open porosity and provide objects with high specific area. However, La and Fe do not form any perovskite structure when the particle gets oxidized in the air after evaporation of liquid nitrogen.

There is still way to improve the control of the process. PVD deposition of La and Fe, followed by an appropriate oxidative heat treatment to form the perovskite structure $LaFeO_3$ before erosion might help to keep this structure in the synthesized particles. A controlled post-oxidation process, instead of spontaneous air oxidation, could also be used to better orientate the formation of oxides.

5. References

[1] A.V. Nominé, N. Tarasenka, A. Nevar *et al.*, Plasma Phys. Control. Fusion, **64**, 014003, (2021).
[2] A. Hamdan, C. Noel, J. Ghanbaja *et al.*, Mater. Chem. Phys., **142**, 199, (2013).
[3] H. Kabbara, J. Ghanbaja, A. Redjaïmia *et al.*, J. Applied Cryst., **52**, 304, (2019).
[4] N. Tarasenka, A. Nominé, A. Nevar *et al.*, Phys. Rev. Appl., **13**, 014021, (2020).
[5] A. O. Larin, A. Nominé, E. I. Ageev *et al.*, Nanoscale, **12**, 1013, (2020).
[6] V. Guigoz, L. Balan, A. Aboulaich *et al.*, Int. J. Hydrog. Energy, **45**, 17468, (2020).
[7] K.D. Hermanson, S.O. Lumsdon, J.P. Williams *et al.*, Science, **294**, 1082, (2001).
[8] M. Trad, A. Nominé, Natalie Tarasenka *et al.*, Front. Chem. Sci. Eng., **13**, 360, (2019).
[9] A. Hamdan, C. Noël, J. Ghanbaja *et al.*, Mater. Chem. Phys. **142**, 199, (2013).
[10] H. Kabbara, J. Ghanbaja, C. Noël *et al.*, Nano-Struct. Nano-Objects, **10**, 22, (2017).